

æ

Submitted to Computer Physics Communications

February 9, 2020

# Quantum Computer Emulator

Hans De Raedt<sup>1</sup>, Anthony H. Hams<sup>1</sup>, and Kristel Michielsen<sup>2</sup>

<sup>1</sup>*Institute for Theoretical Physics and Materials Science Centre*

<sup>2</sup>*Laboratory for Biophysical Chemistry*

*University of Groningen, Nijenborgh 4*

*NL-9747 AG Groningen, The Netherlands*

E-mail: deraedt@phys.rug.nl, A.H.Hams@phys.rug.nl

E-mail: K.F.L.Michielsen@chem.rug.nl

<http://rugth30.phys.rug.nl/compphys>

Koen De Raedt

*European Marketing Support, Vlasakker 21*

*B-2160 Wommelgem, Belgium*

E-mail: csg8042@wing.rug.nl

We describe a quantum computer emulator for a generic, general purpose quantum computer. This emulator consists of a simulator of the physical realization of the quantum computer and a graphical user interface to program and control the simulator. We illustrate the use of the quantum computer emulator through various implementations of the Deutsch-Jozsa and Grover's database search algorithm.

PACS numbers: 03.67.Lx, 05.30.-d, 89.80.+h, 02.70Lq

## 1. Introduction

Recent progress in the field of quantum information processing has opened new prospects to use quantum mechanical phenomena for processing information. The operation of elementary quantum logic gates using ion traps, cavity QED, and NMR technology has been demonstrated. A primitive Quantum Computer (QC) [1 – 4] and secure quantum cryptographic systems have been build [5 – 7]. Recent theoretical work has shown that a QC has the potential of solving certain computationally hard problems such as factoring integers and searching databases much faster than a conventional computer [8 – 13].

The fact that a QC might be more powerful than an ordinary computer is based on the notion that a quantum system can be in any superposition of states and that

interference of these states allows exponentially many computations to be done in parallel [14]. This intrinsic parallelism might be used to solve other difficult problems as well, such as for example the calculation of the physical properties of quantum many-body systems [15 – 18]. In fact, part of Feynman’s original motivation to consider QC’s was that they might be used as a vehicle to perform exact simulations of quantum mechanical phenomena [19].

Just as simulation is an integral part of the design process of each new generation of microprocessors, software to emulate the physical model representing the hardware implementation of a quantum processor may prove essential. In contrast to conventional digital circuits (which may be built using vacuum tubes, relays, CMOS etc.) where the internal working of each basic unit is irrelevant for the logical operation of the whole machine (but extremely relevant for the speed of operation and the cost of the machine of course), in a QC the internal quantum dynamics of each elementary constituent is a key ingredient of the QC itself. Therefore it is essential to incorporate into a simulation model, the physics of the elementary units that make up the QC.

Theoretical work on quantum computation usually assumes the existence of units that perform highly idealized unitary operations. However, in practice these operations are difficult to realize: Disregarding decoherence, a hardware implementation of a QC will perform unitary operations that are more complicated than those considered in most theoretical work. Therefore it is important to have theoretical tools to validate designs of physically realizable quantum processors.

This paper describes a Quantum Computer Emulator (QCE) to emulate various hardware designs of QC’s. The QCE simulates the physical processes that govern the operation of the hardware quantum processor, strictly according to the laws of quantum mechanics. The QCE also provides an environment to debug and execute quantum algorithms (QA’s) under realistic experimental conditions. This is illustrated for several implementations of the Deutsch-Jozsa [20, 21] and Grover’s database search algorithm [12, 13] on QC’s using ideal and more realistic units, such as those used in the 2-qubit NMR QC [3, 4]. Elsewhere [18] we present results of a QA to compute the thermodynamic properties of quantum many-body systems obtained on a 21-qubit hard-coded version of the QCE. The QCE software runs in a W95/W98/NT4 environment and may be downloaded from <http://rugth30.phys.rug.nl/compphys/qce.htm>.

## 2. QCE: Quantum Computer Emulator

Generically, hardware QC’s are modeled in terms of quantum spins (qubits) that evolve in time according to the time-dependent Schrödinger equation (TDSE)

$$i\frac{\partial}{\partial t}|\Phi(t)\rangle = H(t)|\Phi(t)\rangle \quad , \quad (1)$$

in units such that  $\hbar = 1$  and where

$$|\Phi(t)\rangle = a(\downarrow, \downarrow, \dots, \downarrow; t) |\downarrow, \downarrow, \dots, \downarrow\rangle + a(\uparrow, \downarrow, \dots, \downarrow; t) |\uparrow, \downarrow, \dots, \downarrow\rangle + \dots + a(\uparrow, \uparrow, \dots, \uparrow; t) |\uparrow, \uparrow, \dots, \uparrow\rangle , \quad (2)$$

describes the state of the whole QC at time  $t$ . The complex coefficients  $a(\downarrow, \downarrow, \dots, \downarrow; t), \dots, a(\uparrow, \uparrow, \dots, \uparrow; t)$  completely specify the state of the quantum system. The time-dependent Hamiltonian  $H(t)$  takes the form [22]

$$H(t) = - \sum_{j,k=1}^L \sum_{\alpha=x,y,z} J_{j,k,\alpha}(t) S_j^\alpha S_k^\alpha - \sum_{j=1}^L \sum_{\alpha=x,y,z} (h_{j,\alpha,0}(t) + h_{j,\alpha,1}(t) \sin(f_{j,\alpha}t + \varphi_{j,\alpha})) S_j^\alpha , \quad (3)$$

where the first sum runs over all pairs  $P$  of spins (qubits),  $S_j^\alpha$  denotes the  $\alpha$ -th component of the spin-1/2 operator representing the  $j$ -th qubit,  $J_{j,k,\alpha}(t)$  determines the strength of the interaction between the qubits labeled  $j$  and  $k$ ,  $h_{j,\alpha,0}(t)$  and  $h_{j,\alpha,1}(t)$  are the static (magnetic) and periodic (RF) field acting on the  $j$ -th spin respectively. The frequency and phase of the periodic field are denoted by  $f_{j,\alpha}$  and  $\varphi_{j,\alpha}$ . The number of qubits is  $L$  and the dimension of the Hilbert space  $D = 2^L$ .

Hamiltonian (3) is sufficiently general to capture the salient features of most physical models of QC's. Interactions between qubits that involve different spin components have been left out in (3) because we are not aware of a candidate technology of QC where these would be important. Incorporating these interactions requires some trivial additions to the QCE program.

A QA for the QC modeled by (1) consists of a sequence of elementary operations which we will call micro instructions (MI's) in the sequel. They are not exactly playing the same role as MI's do in digital processors, they merely represent the smallest units of operation the quantum processor can carry out. The action of a MI on the state  $|\Psi\rangle$  of the quantum processor is defined by specifying how long it acts (i.e. the time interval it is active), and the values of all the  $J$ 's and  $h$ 's appearing in (1). The  $J$ 's and  $h$ 's are fixed during the operation of the MI. A MI transforms the input state  $|\Psi(t)\rangle$  into the output state  $|\Psi(t+\tau)\rangle$  where  $\tau$  denotes the time interval during which the MI is active. During this time interval the only time-dependence of  $H(t)$  is through the sinusoidal modulation of the fields on the spins.

According to (2) the time evolution of the QC, i.e. the solution of TDSE (1), is determined by the unitary transformation  $U(t+\tau, t) \equiv \exp_+(-i \int_t^{t+\tau} H(u) du)$ , where  $\exp_+$  denotes the time-ordered exponential function. Using the semi-group property of  $U(t+\tau, t)$  we can write

$$U(t + \tau, t) = U(t + m\delta, t + (m-1)\delta) \cdots U(t + 2\delta, t + \delta)U(t + \delta, t) \quad , \quad (4)$$

where  $\tau = m\delta$  ( $m \geq 1$ ). The standard procedure to construct algorithms for solving the TDSE is to replace each  $U(t + (n+1)\delta, t + n\delta)$  by a symmetrized product-formula approximation [23 – 25]. For the case at hand a convenient choice is (other decompositions [26, 27] work equally well but are somewhat less efficient for our purposes):

$$U(t + (n+1)\delta, t + n\delta) \approx \tilde{U}(t + (n+1)\delta, t + n\delta) \quad , \quad (5a)$$

$$\begin{aligned} \tilde{U}(t + (n+1)\delta, t + n\delta) &= e^{-i\delta H_z(t+(n+1/2)\delta)/2} e^{-i\delta H_y(t+(n+1/2)\delta)/2} \\ &\quad \times e^{-i\delta H_x(t+(n+1/2)\delta)} e^{-i\delta H_y(t+(n+1/2)\delta)/2} \\ &\quad \times e^{-i\delta H_z(t+(n+1/2)\delta)/2} \quad , \end{aligned} \quad (5b)$$

where

$$\begin{aligned} H_\alpha(t) &= - \sum_{j,k=1}^L J_{i,j,\alpha} S_j^\alpha S_k^\alpha \\ &\quad - \sum_{j=1}^L (h_{j,\alpha,0} + h_{j,\alpha,1} \sin(f_{j,\alpha} t + \varphi_{j,\alpha})) S_j^\alpha \quad ; \quad \alpha = x, y, z \quad . \end{aligned} \quad (6)$$

Note that in (6) we have omitted the time dependence of the  $J$ 's and the  $h$ 's to emphasize that these parameters are fixed during the execution of a particular MI.

Evidently  $\tilde{U}(t + \tau, t)$  is unitary by construction, implying that the algorithm to solve the TDSE is unconditionally stable [23]. It can be shown that  $\|U(t + \tau, t) - \tilde{U}(t + \tau, t)\| \leq c\delta^3$ , implying that the algorithm is correct to second order in the time-step  $\delta$  [23]. If necessary,  $\tilde{U}(t + \tau, t)$  can be used as a building block to construct higher-order algorithms [28 – 31]. In practice it is easy to find reasonable values of  $m$  such that the results obtained no longer depend on  $m$  (and  $\delta$ ). Then, for all practical purposes, these results are indistinguishable from the exact solution of the TDSE (1).

As already indicated above, as basis states  $\{|\phi_n\rangle\}$  we take the direct product of the eigenvectors of the  $S_j^z$  (i.e. spin-up  $|\uparrow\rangle_j$  and spin-down  $|\downarrow\rangle_j$ ). In this basis  $e^{-i\delta H_z(t+(n+1/2)\delta)/2}$  changes the input state by altering the phase of each of the basis vectors. As  $H_z$  is a sum of pair interactions it is trivial to rewrite this operation as a direct product of 4x4 diagonal matrices (containing the interaction-controlled phase shifts) and 4x4 unit matrices. Hence the computation of  $\exp(-i\delta H_z(t+(n+1/2)\delta)/2)|\Psi\rangle$  has been reduced to the multiplication of two vectors, element-by-element. The QCE carries out  $\mathcal{O}(P2^L)$  operations to perform this calculation but a

real QC operates on all qubits simultaneously and would therefore only need  $\mathcal{O}(P)$  operations.

Still working in the same representation, the action of  $e^{-i\delta H_y(t+(n+1/2)\delta)/2}$  can be written in a similar manner but the matrices that contain the interaction-controlled phase-shift have to be replaced by non-diagonal matrices. Although this does not present a real problem it is more efficient and systematic to proceed as follows. Let us denote by  $\mathcal{X}$  ( $\mathcal{Y}$ ) the rotation by  $\pi/2$  of all spins about the  $x(y)$ -axis. As

$$\begin{aligned} e^{-i\delta H_y(t+(n+1/2)\delta)/2} &= \mathcal{X} \mathcal{X}^\dagger e^{-i\delta H_y(t+(n+1/2)\delta)/2} \mathcal{X} \mathcal{X}^\dagger \\ &= \mathcal{X} e^{-i\delta H'_z(t+(n+1/2)\delta)/2} \mathcal{X}^\dagger , \end{aligned} \quad (7)$$

it is clear that the action of  $e^{-i\delta H_y(t+(n+1/2)\delta)/2}$  can be computed by applying to each qubit, the inverse of  $\mathcal{X}$  followed by an interaction-controlled phase-shift and  $\mathcal{X}$ . The prime in (7) indicates that  $J_{i,j,z}$ ,  $h_{i,z,0}$ ,  $h_{i,z,0}$  and  $f_{i,z}$  in  $H_z(t+(n+1/2)\delta)$  have to be replaced by  $J_{i,j,y}$ ,  $h_{i,y,0}$ ,  $h_{i,y,0}$  and  $f_{i,y}$  respectively. A similar procedure is used to compute the action of  $e^{-i\delta H_x(t+(n+1/2)\delta)}$ : We only have to replace  $\mathcal{X}$  by  $\mathcal{Y}$ . The operation counts for  $e^{-i\delta H_x(t+(n+1/2)\delta)}$  (or  $e^{-i\delta H_y(t+(n+1/2)\delta)/2}$ ) are  $\mathcal{O}((P+2)2^L)$  and  $\mathcal{O}(P+2)$  for the QCE and QC respectively. On a QC the total operation count per time-step is  $\mathcal{O}(3P+4)$ .

### 3. Graphical User Interface

The QCE consists of a QC simulator, described above, and a graphical user interface (GUI) that controls the former. The GUI considerably simplifies the task of specifying the MI's (i.e. to model the hardware) and to execute quantum programs (QP's). The QCE runs in a Windows 95/98/NT environment. Using the GUI is very much like working with any other standard MS-Windows application. The maximum number of qubits in the version of the QCE that is available for distribution is limited to eight. The QCE is distributed as a self-installing executable, containing the program, documentation, and all the QP's discussed in this paper. These QP's also illustrate the use of the GUI itself.

Some of the salient features of the GUI of the QCE are shown in figs.1-4. The main window contains a window that shows the set of MI's that is currently active and several other windows (limited to 10) that contain QPs. Help on a button appears when the mouse moves over the button, a standard Windows feature.

Writing a QA on the QCE from scratch is a two-step process. First one has to specify the MI's, taking into account the particular physical realization of the QC that one wants to emulate. The "MI" window offers all necessary tools to edit (see Fig.2) and manipulate (groups of) MI's. The second step, writing a QP, consists of dragging and dropping MI's onto a "QP" window.

Each MI set has two reserved MI's: A break point (allowing the QP to pause

at a specified point) and a MI to initialize the QC. Normally the latter is the first instruction in a QP. Each QP window has a few buttons to control the operation of the QC.

The results of executing a QP appear in color-coded form at the bottom of the corresponding program window. For each qubit the expectation value of the three spin components are shown:  $Q_j^\alpha \equiv 1/2 - \langle S_j^\alpha \rangle$  ( $\alpha = x, y, z$ ) green corresponds to 0, red to 1. Usually only one row of values (the  $z$ -component) will be of interest. Optionally the QCE will generate text files with the numerical results for further processing.

The QCE supports the use of QP's as MI's (see Figs.3,4). QP's can be added to a particular MI set through the button labeled "QP". During execution, a QP that is called from another QP will call either another QP or a genuine MI from the currently loaded set of MI's. The QCE will skip all initialization MI's except for the first one. This facilitates the testing of QP that are used as sub-QP's. A QP calling a MI that cannot be found in the current MI set will generate an error message and stop.

## 4. Applications

Our aim is to illustrate how to use the QCE to simulate the QC implemented using NMR techniques [1, 2, 3, 4]. A classical coin has been used to decide which of the two realizations (i.e. [1, 2] or [3, 4]) to take as an example. In the NMR experiments [3, 4] the two nuclear spins of the ( $^1\text{H}$  and  $^{13}\text{C}$  atoms in a carbon-13 labeled chloroform) molecule are placed in a strong static magnetic field in the  $+z$  direction. In the absence of interactions with other degrees of freedom this spin-1/2 system can be modeled by the hamiltonian

$$H = -J_{1,2,z}S_1^zS_2^z - h_{1,z,0}S_1^z - h_{2,z,0}S_2^z , \quad (8)$$

where  $h_{1,z,0}/2\pi \approx 500\text{MHz}$ ,  $h_{2,z,0}/2\pi \approx 125\text{MHz}$ , and  $J_{1,2,z}/2\pi \approx -215\text{Hz}$  [3]. As the antiferromagnetic interaction between the spins is much weaker than the coupling to the external field and (8) is a diagonal matrix with respect to the basis states chosen, the ground state of (8) is the state with the two spins up. Following [3] we denote this state by  $|00\rangle = |0\rangle \otimes |0\rangle = |\uparrow\uparrow\rangle$ , i.e. the state with spin up corresponds to a qubit  $|0\rangle$ . A state of the  $N$ -qubit QC will be denoted by  $|x_1x_2\dots x_N\rangle = |x_1\rangle \otimes |x_2\rangle \dots |x_N\rangle$ .

It is expedient to write the TDSE for this problem in frames of reference rotating with the nuclear spin. Formally this is accomplished by substituting in (1)

$$|\Phi(t)\rangle = e^{it(h_{1,z,0}S_1^z + h_{2,z,0}S_2^z)}|\Psi(t)\rangle , \quad (9)$$

so that in the absence of RF-fields the time evolution of  $\Psi(t)$  is governed by the

hamiltonian  $H = -J_{1,2,z}S_1^zS_2^z$ .

This transformation removes from the sequence of elementary operations, phase factors that are irrelevant for the value of the qubits. Indeed, as the expectation value of a qubit is related to the expectation value of the  $z$  component of the spin:

$$Q_j \equiv Q_j^z = \frac{1}{2} - \langle \Phi(t) | S_i^z | \Phi(t) \rangle \quad , \quad (10a)$$

and

$$\begin{aligned} \langle \Phi(t) | S_j^z | \Phi(t) \rangle &= \langle \Psi(t) | e^{-it(h_{1,z,0}S_1^z + h_{2,z,0}S_2^z)} S_j^z e^{it(h_{1,z,0}S_1^z + h_{2,z,0}S_2^z)} | \Psi(t) \rangle \\ &= \langle \Psi(t) | S_j^z | \Psi(t) \rangle \quad . \end{aligned} \quad (10b)$$

From (10) it is clear that transformation (9) has no net effect. This is not the case for the expectation values of the  $x$  or  $y$  component of the spins: The phase factors induce an oscillatory behavior, reflecting the fact that the spins are rotating about the  $z$ -axis (see (A.17) for an example). In the following it is implicitly assumed that the basis states of the spins refer to states in the corresponding rotating frame.

We now discuss the implementation on the QCE of two QA's that have been tested on an NMR QC [3, 4].

#### 4.1 Deutsch-Jozsa algorithm

This QA [20, 32] and its refinement [21] provide illustrative examples of how the intrinsic parallelism of a QC can be exploited to solve certain decision problems.

Consider a function  $f = f(x_1, x_2, \dots, x_N) = 0, 1$  that transforms the  $N$  bits  $\{x_n = 0, 1\}$  to one output bit. There are three classes of functions  $f$ : *Constant* functions, returning 0 or 1 independent of the input  $\{x_n\}$ , *balanced* functions that give  $f = 0$  for exactly half of the  $2^N$  possible inputs and  $f = 1$  for the remaining inputs, and *other* functions that do not belong to one of the two other classes. Some examples of *constant* and *balanced* functions are given in tables 1 and 2.

The Deutsch-Jozsa (D-J) algorithm allows a QC to decide whether a function is *constant* or *balanced*, given the additional piece of information that functions of the type *other* will not be fed into the QC. For a function of one input variable the D-J problem is equivalent to the problem of deciding if a coin is fair (has head and tail) or fake (e.g. two heads). In the case of the coin we would have to look at both sides to see if it is fair. A QC can make a decision by looking only once (at the two sides simultaneously).

In the NMR experiment the two qubits of the QC (i.e. the two nuclear spins of the chloroform molecule) are used during the execution of the D-J algorithm although in principle only one qubit would do [21]. However our aim is to simulate the NMR-QC experiment and therefore we will closely follow Ref. [3]. Accordingly the first qubit is considered as the input variable, the other one serves as work

Table 1. Input and output values of *constant* ( $f_1(x)$ ,  $f_2(x)$ ) and *balanced* functions ( $f_3(x)$ ,  $f_4(x)$ ) of one input bit  $x$ .

$x$	$f_1(x)$	$f_2(x)$	$f_3(x)$	$f_4(x)$
0	0	1	0	1
1	0	1	1	0

Table 2. Input and output values of *constant* ( $f_1(x)$ ,  $f_2(x)$ ) and *balanced* functions ( $f_3(x)$ ,  $f_4(x)$ ,  $f_5(x)$ ) of three input bits  $x = \{x_1, x_2, x_3\}$ . Note that  $f_4(x)$  only depends on  $x_2$  and is therefore rather trivially *balanced*.

$x_1$	$x_2$	$x_3$	$f_1(x_1, x_2, x_3)$	$f_2(x_1, x_2, x_3)$	$f_3(x_1, x_2, x_3)$	$f_4(x_1, x_2, x_3)$	$f_5(x_1, x_2, x_3)$
0	0	0	0	1	0	0	0
1	0	0	0	1	0	0	1
0	1	0	0	1	0	1	1
1	1	0	0	1	1	1	0
0	0	1	0	1	0	0	1
1	0	1	0	1	1	0	0
0	1	1	0	1	1	1	0
1	1	1	0	1	1	1	1

Table 3. Results of letting the sequences  $F_1, \dots, F_3$  (see (12)) transform the four basis states. Inspection of the outputs demonstrated that these sequences implement the *constant* or *balanced* functions of Table 1.

$x$	$ \Psi\rangle$	$F_1 \Psi\rangle$	$F_2 \Psi\rangle$	$F_3 \Psi\rangle$	$F_4 \Psi\rangle$
0	$ 00\rangle$	$- 00\rangle$	$i 01\rangle$	$e^{-i\pi/4} 00\rangle$	$-e^{+i\pi/4} 01\rangle$
1	$ 10\rangle$	$- 10\rangle$	$i 11\rangle$	$-e^{-i\pi/4} 11\rangle$	$e^{+i\pi/4} 10\rangle$
2	$ 01\rangle$	$- 01\rangle$	$i 00\rangle$	$e^{-i\pi/4} 01\rangle$	$-e^{+i\pi/4} 00\rangle$
3	$ 11\rangle$	$- 11\rangle$	$i 10\rangle$	$-e^{-i\pi/4} 10\rangle$	$e^{+i\pi/4} 11\rangle$

space.

Before the actual calculation starts the QC has to be initialized. This amounts to setting each of the two qubits to  $|0\rangle$ . On the QCE this is accomplished by the MI “Initialize”, a reserved MI name in the QCE (see above). The first step in the D-J algorithm is to prepare the QC by putting the first qubit in the state  $(|0\rangle + |1\rangle)/\sqrt{2}$  and the second one in  $(|0\rangle - |1\rangle)/\sqrt{2}$  [3]. This can be done by performing two rotations:

Table 4. Specification of the micro instructions implementing the two-qubit NMR QC on the QCE. Frequencies have been rescaled such that  $h_{j,\alpha,0} = 1$  corresponds to 500MHz. The execution time of each micro instruction is given by the second row ( $\tau/2\pi$ ). The inverse of e.g.  $\bar{X}_1$  is found by reversing the sign of  $h_{1,x,1}$ . Note that the QCE is constructed such that a rotation about the  $x(y)$  axis requires a RF-pulse along the  $y(x)$  direction (see Appendix A).

Parameter	$X_1$	$\bar{X}_2$	$Y_1$	$\bar{Y}_2$	$I(\pi/2)$	$I(\pi)$
$\tau/2\pi$	10	40	10	40	$25 \times 10^4$	$50 \times 10^4$
$J_{1,2,z}$	$-10^{-6}$	$-10^{-6}$	$-10^{-6}$	$-10^{-6}$	$-10^{-6}$	$-10^{-6}$
$h_{1,x,0}$	0	0	0	0	0	0
$h_{2,x,0}$	0	0	0	0	0	0
$h_{1,y,0}$	0	0	0	0	0	0
$h_{2,y,0}$	0	0	0	0	0	0
$h_{1,z,0}$	1	1	1	1	1	1
$h_{2,z,0}$	0.25	0.25	0.25	0.25	0.25	0.25
$h_{1,x,1}$	0	0	0.05	-0.05	0	0
$h_{2,x,1}$	0	0	0.0125	-0.0125	0	0
$f_{1,x}$	0	0	1	0.25	0	0
$f_{2,x}$	0	0	1	0.25	0	0
$\varphi_{1,x}$	0	0	0	0	0	0
$\varphi_{2,x}$	0	0	0	0	0	0
$h_{1,y,1}$	-0.05	0.05	0	0	0	0
$h_{2,y,1}$	-0.0125	0.0125	0	0	0	0
$f_{1,y}$	1	0.25	0	0	0	0
$f_{2,y}$	1	0.25	0	0	0	0
$\varphi_{1,y}$	0	0	0	0	0	0
$\varphi_{2,y}$	0	0	0	0	0	0
$h_{1,z,1}$	0	0	0	0	0	0
$h_{2,z,1}$	0	0	0	0	0	0
$f_{1,z}$	0	0	0	0	0	0
$f_{2,z}$	0	0	0	0	0	0
$\varphi_{1,z}$	0	0	0	0	0	0
$\varphi_{2,z}$	0	0	0	0	0	0

$$\text{Prepare} \Leftrightarrow \bar{Y}_2 Y_1 \quad , \quad (11)$$

where  $Y_j$  represents the operation of rotating **clock-wise** the spin  $j$  by  $\pi/2$  along the  $y$  axis, and  $\bar{Y}_j$  its inverse (see Appendix A). In this paper we adopt the convention that all expressions like (11) have to be read from **right to left**.

Table 5. Final state of the QC after running the D-J algorithm for the case of the ideal QC ( $Q_1, Q_2$ , see table 5) and the NMR-QC ( $\hat{Q}_1, \hat{Q}_2$ , see table 4). The results ( $\tilde{Q}_1, \tilde{Q}_2$ ) have been obtained by modifying the NMR MI's such that the RF-pulses only affect the spin that is in resonance. The last two rows show the results of running the refined version [21] of the D-J algorithm.  $\mathcal{Q}_1$  : Ideal operations  $\hat{\mathcal{Q}}_1$  : NMR implementation.

	$f_1(x)$	$f_2(x)$	$f_3(x)$	$f_4(x)$
$Q_1$	0.000	0.000	1.000	1.000
$Q_2$	0.000	0.000	0.000	0.000
$\hat{Q}_1$	0.169	0.064	0.867	0.867
$\hat{Q}_2$	0.999	1.000	0.001	0.002
$\tilde{Q}_1$	0.000	0.000	0.998	0.998
$\tilde{Q}_2$	1.000	1.000	0.001	0.001
$\hat{\mathcal{Q}}_1$	0.000	0.000	1.000	1.000
$\mathcal{Q}_1$	0.000	0.000	0.995	0.996

Table 6. Specification of the micro instructions implementing a mathematically perfect two-qubit QC on the QCE. The execution time of each micro instruction is given by the second row ( $\tau/2\pi$ ). The inverse of e.g.  $\bar{X}_1$  is found by reversing the sign of  $h_{1,x,0}$ . Model parameters omitted are zero for all micro instructions.

Parameter	$X_1$	$\bar{X}_2$	$Y_1$	$\bar{Y}_2$	$I(\pi/2)$	$I(\pi)$
$\tau/2\pi$	0.25	0.25	0.25	0.25	$25 \times 10^4$	$50 \times 10^4$
$J_{1,2,z}$	0	0	0	0	$-10^{-6}$	$-10^{-6}$
$h_{1,x,0}$	+1	0	0	0	0	0
$h_{2,x,0}$	0	-1	0	0	0	0
$h_{1,y,0}$	0	0	+1	0	0	0
$h_{2,y,0}$	0	0	0	-1	0	0

The next step is to compute the function  $f(x)$ . Following [3] the two *constant* and two *balanced* functions listed in Table 1 can be implemented by the sequences

$$f_1(x) \Leftrightarrow F_1 = X_2 X_2 I(\pi/2) X_2 X_2 I(\pi/2) \quad , \quad (12a)$$

$$f_2(x) \Leftrightarrow F_2 = I(\pi/2) X_2 X_2 I(\pi/2) \quad , \quad (12b)$$

$$f_3(x) \Leftrightarrow F_3 = Y_1 \bar{X}_1 \bar{Y}_1 X_2 \bar{Y}_2 I(\pi) Y_2 \quad , \quad (12c)$$

$$f_4(x) \Leftrightarrow F_4 = Y_1 \bar{X}_1 \bar{Y}_1 X_2 \bar{Y}_2 I(\pi) Y_2 \quad , \quad (12d)$$

where  $X_j$  denotes the **clock-wise** rotation of spin  $j$  by  $\pi/2$  along the  $x$  axis,  $\bar{X}_j$  the inverse operation and  $I(a) \equiv e^{-iaS_1^zS_2^z}$  represents the time evolution due to  $H$  itself. In Table 3 we show the result of letting the sequences (12) act on the basis states. It is clear that they have the desired properties. Note that prefactors have no physical relevance (they drop out when we compute expectation values) and that  $F_1$  is a rather complicated version of the identity operation.

Finally there is a read-out operation which corresponds to in the inverse of the “Prepare”:

$$\text{ReadOut} \Leftrightarrow \bar{Y}_1 Y_2 \quad . \quad (13)$$

Note that there is some flexibility in the choice of these sequences. For instance to “Prepare” we could have used Walsh-Hadamard (WH) transformations  $W_1 W_2$  as well.

Upto this point the D-J algorithm has been written as a sequence of unitary operations that perform specific tasks. Now we consider two different implementations of these unitary transformations: The first one will be physical, i.e. we will use the QCE simulate the NMR-QC experiment itself. The second will be “computer-science” like, i.e. we will use highly idealized, non-realizable rotations.

NMR uses radiofrequency electromagnetic pulses to rotate the spins [33, 34]. By tuning the frequency of the RF-field to the precession frequency of a particular spin, the power of the applied pulse (= intensity times duration) controls how much the spin will rotate. The axis of the rotation is determined by the direction of the applied RF-field (see [33, 34] or Appendix A). A possible choice of the model parameters, corresponding to the actual experimental values of these parameters, is given in Table 4. For simplicity all frequencies have been normalized with respect to the largest one (i.e. 500MHz in the experiments [3, 4]). Also note that it is convenient to express execution times in units of  $2\pi$ , the default setting in the QCE.

The results of running the QCE with the MI’s simulating the NMR experiment are summarized in Fig.1. The first qubit ( $Q_j = 1/2 - \langle S_j^z \rangle$ ) unambiguously tells us that the functions  $f_1(x)$  and  $f_2(x)$  are constant and that  $f_3(x)$  and  $f_4(x)$  are balanced. Clearly the QCE qualitatively reproduces the experimental results. In the D-J algorithm the final state of the second qubit is irrelevant. In the final state the numerical value of qubit 1, is only approximately zero or one (see Table 5). This is a direct consequence of the fact that we are simulating a genuine physical system.

In an NMR experiment, application of a RF-pulse affects all spins in the sample. Although the response of a spin to the RF-field will only be large when this spin is at resonance, the state of the spins that are not in resonance will also change. These unitary transformations not necessarily commute with the sequence of unitary transformations that follow and may therefore affect the final outcome of the whole computation. Furthermore the use of a time-dependent external field to ro-

tate spins is only an approximation to the simple rotations envisaged in theoretical work (see Appendix A). This definitely has an effect on the expectation values of the spin operators.

With the QCE it is very easy to make a detailed comparison between physical and idealized implementations of QC's: We simply replace the set of MI's ("NMR") by another one ("Ideal", or "NMR-Ideal") and re-run the QP's by simply clicking on the execute buttons. The model parameters we have chosen to implement the "ideal" operations are listed in Table 6. The set "NMR-Ideal" is a copy of "NMR" (see Table 4) except that the RF-pulses only affect the spin that is in resonance, i.e. all operations on qubit  $j$  have  $h_{2,x,j} = h_{2,y,j} = 0$ .

The results of executing the QA's for the "Ideal" case are shown in Fig.2. In the final state the qubits are exactly  $|0\rangle$  or  $|1\rangle$ , as expected. The state of the second qubit not always matches the corresponding state of Fig.1. As mentioned above this is due to the approximate nature of the operations used in the NMR case, but as the final state of the second qubit is irrelevant for the D-J algorithm there is no problem. In Table 5 we collect the numerical values of the qubits as obtained by running the D-J algorithm on the NMR and ideal QC. It is clear in that all cases the D-J algorithm gives the correct answer.

## 4.2 Collins-Kim-Holton algorithm

From the description of the DJ algorithm of one variable ([3], Fig.1) it is evident that the second qubit is redundant because the function call (step T2 in [3]) leaves the state of the second qubit, i.e. the work space, untouched. A refined version of the D-J algorithm (for an arbitrary number of qubits) that does not require a bit for the evaluation of the function is given in [21]. For one variable, the QC has to compute the function

$$f_j \Leftrightarrow \sum_{x=0}^1 (-1)^{f_j(x)} |x\rangle \quad . \quad (14)$$

Following [21] this may be accomplished via an  $f$ -controlled gate defined by

$$U_f |x\rangle = (-1)^{f(x)} |x\rangle \quad . \quad (15)$$

Accordingly, once choice (there are several) of the set of sequences that implements the refined version of the D-J algorithm reads:

$$\text{Prepare} \Leftrightarrow \bar{Y}_1 \quad , \quad (16a)$$

$$f_1(x) \Leftrightarrow F_1 = W_1 W_1 \quad , \quad (16b)$$

$$f_2(x) \Leftrightarrow F_2 = X_1 X_1 \quad , \quad (16c)$$

$$f_3(x) \Leftrightarrow F_3 = \bar{Y}_1 X_1 Y_1 \bar{Y}_1 X_1 Y_1 \quad , \quad (16d)$$

$$f_4(x) \Leftrightarrow F_4 = Y_1 \bar{X}_1 \bar{Y}_1 Y_1 \bar{X}_1 \bar{Y}_1 \quad , \quad (16e)$$

$$\text{ReadOut} \Leftrightarrow \bar{Y}_1 \quad , \quad (16f)$$

The results of running these QP's on the QCE are given in Table 6. It is clear that the refined version performs as expected.

#### 4.3 Grover's database search algorithm

On a conventional computer finding a particular entry in an unsorted list of  $N$  elements requires of the order of  $N$  operations. Grover has shown that a QC can find the item using only  $\mathcal{O}(\sqrt{N})$  attempts [11, 12]. Consider the extremely simple case of a database containing four items and functions  $g_j(x)$ ,  $j = 0, \dots, 3$  that upon query of the database return minus one if  $x = j$  and plus one if  $x \neq j$ . Assuming a uniform probability distribution for the item to be in one of the four locations, the average number of queries required by a conventional algorithm is  $9/4$ . With Grover's QA the correct answer can be found in a single query (this result only holds for a database with 4 items). Grover's algorithm for the four-item database can be implemented on a two-qubit QC.

The key ingredient of Grover's algorithm is an operation that replaces each amplitude of the basis states in the superposition by two times the average amplitude minus the amplitude itself. This operation is called "inversion about the mean" and amplifies the amplitude of the basis state that represents the searched-for item. To see how this works it is useful to consider an example. Let us assume that the item to search for corresponds to e.g. number 2 ( $g_2(0) = g_2(1) = g_2(3) = 1$  and  $g_2(2) = -1$ ). Using the binary representation of integers with the order of the bits reversed, the QC is in the state (up to an irrelevant phase factor as usual)

$$|\Psi\rangle = \frac{1}{2}(|00\rangle + |10\rangle - |01\rangle + |11\rangle) \quad . \quad (17)$$

We return to the question of how to prepare this state below. The operator  $D$  that inverts states like (17) about their mean reads

$$D = \frac{1}{2} \begin{pmatrix} -1 & 1 & 1 & 1 \\ 1 & -1 & 1 & 1 \\ 1 & 1 & -1 & 1 \\ 1 & 1 & 1 & -1 \end{pmatrix} ; \begin{array}{c} |00\rangle \\ |10\rangle \\ |01\rangle \\ |11\rangle \end{array} . \quad (18)$$

The mean amplitude of (17) is  $1/4$  and we find that

$$D|\Psi\rangle = |01\rangle \quad , \quad (19a)$$

i.e. the correct answer, and

$$D^2|\Psi\rangle = \frac{1}{2}(|00\rangle + |10\rangle + |01\rangle + |11\rangle) \quad , \quad (19b)$$

$$D^3|\Psi\rangle = -\frac{1}{2}(|00\rangle + |10\rangle - |01\rangle + |11\rangle) = -|\Psi\rangle \quad , \quad (19c)$$

showing that (in the case of 2 qubits) the correct answer (i.e. the absolute value of the amplitude of  $|10\rangle$  equal to one) is obtained after 1, 4, 7, ... iterations. In general, for more than two qubits, more than one application of  $D$  is required to get the correct answer. In this sense the 2-qubit case is somewhat special.

The next task is to express the preparation and query steps in terms of elementary rotations. For illustrative purposes we stick to the example used above. Initially we set the QC in the state  $|00\rangle$ , i.e. the state with both spins up [35]. and then transform  $|00\rangle$  to the linear superposition (17) by a two-step process. First we set the QC in the uniform superposition state  $|U\rangle$ :

$$\text{Prepare} \Leftrightarrow |U\rangle \equiv W_1 W_2 |00\rangle = -\frac{1}{2}(|00\rangle + |10\rangle + |01\rangle + |11\rangle) \quad , \quad (20)$$

where

$$W_j = X_j X_j \bar{Y}_j = -\bar{X}_j \bar{X}_j \bar{Y}_j = \frac{i}{\sqrt{2}} \begin{pmatrix} 1 & 1 \\ 1 & -1 \end{pmatrix}_j \quad , \quad (21)$$

is the WH tranform on qubit  $j$  which transforms  $|0\rangle$  to  $i(|0\rangle + |1\rangle)/\sqrt{2}$  (see Appendix A). The transformation that corresponds to the application of  $g_2(x)$  to the uniform superposition state is

$$F_2 = \begin{pmatrix} 1 & 0 & 0 & 0 \\ 0 & 1 & 0 & 0 \\ 0 & 0 & -1 & 0 \\ 0 & 0 & 0 & 1 \end{pmatrix} ; \begin{pmatrix} |00\rangle \\ |10\rangle \\ |01\rangle \\ |11\rangle \end{pmatrix} . \quad (22)$$

This transformation can be implemented by first letting the system evolve in time:

$$\begin{aligned} I(\pi)|U\rangle &= e^{-i\pi S_1^z S_2^z} \left[ \frac{1}{2}(|00\rangle + |10\rangle + |01\rangle + |11\rangle) \right] \\ &= \frac{1}{2}(e^{-i\pi/4}|00\rangle + e^{+i\pi/4}|10\rangle + e^{+i\pi/4}|01\rangle + e^{-i\pi/4}|11\rangle) \end{aligned} \quad (23)$$

For the NMR-QC based on hamiltonian (8) this means letting the system evolve in time (without applying pulses) for a time  $\tau_0 = -\pi/J_{1,2,z}$  (recall  $J_{1,2,z} < 0$ ). Next we apply a sequence of single-spin rotations to change the four phase factors such that we get the desired state. The two sequences  $YX\bar{Y}$  and  $Y\bar{X}\bar{Y}$  (see Appendix B) are particulary useful for this purpose. We find

$$\begin{aligned}
& Y_1 X_1 \bar{Y}_1 Y_2 \bar{X}_2 \bar{Y}_2 \left[ \frac{1}{2} (e^{-i\pi/4} |00\rangle + e^{+i\pi/4} |10\rangle + e^{+i\pi/4} |01\rangle + e^{-i\pi/4} |11\rangle) \right] \\
& = \frac{1}{2} (e^{-i\pi/4} |00\rangle + e^{-i\pi/4} |10\rangle + e^{+3i\pi/4} |01\rangle + e^{-i\pi/4} |11\rangle) \\
& = \frac{e^{-i\pi/4}}{2} (|00\rangle + |10\rangle - |01\rangle + |11\rangle) . \tag{24}
\end{aligned}$$

Combining (23) and (24) we can construct the sequence  $G_j$  that transforms the uniform superposition  $|U\rangle$  to the state that corresponds to  $g_j(x)$ :

$$F_0 = Y_1 X_1 \bar{Y}_1 Y_2 X_2 \bar{Y}_2 I(\pi) , \tag{25a}$$

$$F_1 = Y_1 \bar{X}_1 \bar{Y}_1 Y_2 X_2 \bar{Y}_2 I(\pi) , \tag{25b}$$

$$F_2 = Y_1 X_1 \bar{Y}_1 Y_2 \bar{X}_2 \bar{Y}_2 I(\pi) , \tag{25c}$$

$$F_3 = Y_1 \bar{X}_1 \bar{Y}_1 Y_2 \bar{X}_2 \bar{Y}_2 I(\pi) . \tag{25d}$$

The remaining task is to express the operation of inversion about the mean, i.e. the matrix  $D$  (see (18)), by a sequence of elementary operations. It is not difficult to see that  $D$  can be written as the product of a WH transform, a conditional phase shift  $P$  and another WH transform:

$$\begin{aligned}
D &= W_1 W_2 P W_1 W_2 \\
&= W_1 W_2 \begin{pmatrix} 1 & 0 & 0 & 0 \\ 0 & -1 & 0 & 0 \\ 0 & 0 & -1 & 0 \\ 0 & 0 & 0 & -1 \end{pmatrix} W_1 W_2 . \tag{26a}
\end{aligned}$$

The same approach that was used to implement  $g_2(x)$  also works for the conditional phase shift  $P$  ( $= -F_0$ ) and yields

$$P = Y_1 X_1 \bar{Y}_1 Y_2 X_2 \bar{Y}_2 I(\pi) . \tag{27}$$

The complete sequence  $U_j$  reads

$$U_j = W_1 W_2 P W_1 W_2 F_j . \tag{28}$$

Each sequence  $U_j$  can be shortened by observing that in some cases a rotation is followed by its inverse. Making use of the alternative representations of the WH transform  $W_i$  (see (Appendix B)), the sequence for e.g.  $j = 2$  can be written as

$$\begin{aligned}
W_1 W_2 F_2 &= - \bar{X}_1 \bar{X}_1 \bar{Y}_1 X_2 X_2 \bar{Y}_2 Y_1 X_1 \bar{Y}_1 Y_2 \bar{X}_2 \bar{Y}_2 I(\pi) \\
&= - \bar{X}_1 \bar{Y}_1 X_2 \bar{Y}_2 I(\pi) . \tag{29}
\end{aligned}$$

Table 7. Final state of the QC after running the Grover's database search algorithm for the case of the ideal QC ( $Q_1, Q_2$ , see table 5) and the NMR-QC ( $\hat{Q}_1, \hat{Q}_2$ , see table 4).

	$g_0(x)$	$g_1(x)$	$g_2(x)$	$g_3(x)$
$Q_1$	0	1	0	1
$Q_2$	0	0	1	1
$\hat{Q}_1$	0.045	0.963	0.035	0.972
$\hat{Q}_2$	0.171	0.164	0.829	0.837

The sequences for the other cases can be shortened as well, yielding

$$U_0 = \bar{X}_1 \bar{Y}_1 \bar{X}_2 \bar{Y}_2 I(\pi) \bar{X}_1 \bar{Y}_1 \bar{X}_2 \bar{Y}_2 I(\pi) , \quad (30a)$$

$$U_1 = \bar{X}_1 \bar{Y}_1 \bar{X}_2 \bar{Y}_2 I(\pi) X_1 \bar{Y}_1 \bar{X}_2 \bar{Y}_2 I(\pi) , \quad (30b)$$

$$U_2 = \bar{X}_1 \bar{Y}_1 \bar{X}_2 \bar{Y}_2 I(\pi) \bar{X}_1 \bar{Y}_1 X_2 \bar{Y}_2 I(\pi) , \quad (30c)$$

$$U_3 = \bar{X}_1 \bar{Y}_1 \bar{X}_2 \bar{Y}_2 I(\pi) X_1 \bar{Y}_1 X_2 \bar{Y}_2 I(\pi) , \quad (30d)$$

where in  $U_1$  and  $U_2$  a physically irrelevant sign has been dropped. Note that the binary representation of  $x$  translates into the presence (0) or absence (1) in (30) of a bar on the rightmost  $X_1$  and  $X_2$ .

As before, our aim is to use the QCE to simulate the NMR-QC experiment [4]. For the D-J algorithm we already specified the physical parameters for the elementary operations and we will make use of the same set of MI's here. In Figs.3 and 4 we show the QCE after running the four cases  $g_0(x), \dots, g_3(x)$  using the ideal (Fig.3) and NMR (Fig.4) MI's. The numerical values of the qubits in the final state are given in Table 7. In both cases the QA performs as it should. In the ideal case, the final state of the QC is exactly equal to  $|x\rangle$  (binary representation of integers). Using RF-pulses instead of ideal transformations to perform  $\pi/2$  rotations leads to less certain answers: The final state is no longer a pure basis state but some linear superposition of the four basis states. What is beyond doubt though is that in all cases the weight of  $|x\rangle$  is by far the largest. Hence the QC returns the correct answer.

## 5. Summary

We have described the internal operation of QCE, a the software tool for simulating hardware realizations of quantum computers. The QCE simulates the physical (quantum) processes that govern the operation of the hardware quantum processor by solving the time-dependent Schrödinger equation. The use of the QCE has been illustrated by several implementations of the Deutsch-Jozsa and Grover's database

search algorithm, on QC's using ideal and more realistic units, such as those of 2-qubit NMR-QC's. Currently the QCE is used to study the stability of quantum computers in relation to the non-idealness of realizable elementary operations [36].

## 6. Acknowledgement

Generous support from the Dutch “Stichting Nationale Computer Faciliteiten (NCF)” is gratefully acknowledged.

## Appendix A: Spin-1/2 algebra

Here we present a collection of standard results on spin-1/2 systems which are used in the paper and are taken from [34]. We begin with some notation.

The two basis states spanning the Hilbert space of a two-state quantum system are usually denoted by

$$|\uparrow\rangle \equiv \begin{pmatrix} 1 \\ 0 \end{pmatrix} \quad , \quad |\downarrow\rangle \equiv \begin{pmatrix} 0 \\ 1 \end{pmatrix} \quad . \quad (A.1)$$

The three components of the spin-1/2 operator  $\vec{S}$  acting on this Hilbert space are defined by

$$S^x = \frac{\hbar}{2} \begin{pmatrix} 0 & 1 \\ 1 & 0 \end{pmatrix} \quad , \quad S^y = \frac{\hbar}{2} \begin{pmatrix} 0 & -i \\ i & 0 \end{pmatrix} \quad , \quad S^z = \frac{\hbar}{2} \begin{pmatrix} 1 & 0 \\ 0 & -1 \end{pmatrix} \quad . \quad (A.2)$$

By convention the representation (A.2) is chosen such that  $|\uparrow\rangle$  and  $|\downarrow\rangle$  are eigenstates of  $S^z$  with eigenvalues  $+\hbar/2$  and  $-\hbar/2$  respectively.

From (A.2) it is clear that  $(S^x)^2 = (S^y)^2 = (S^z)^2 = \hbar^2/4$  so that

$$\cos\left(\frac{\varphi S^\alpha}{\hbar}\right) = \cos\left(\frac{\varphi}{2}\right) \begin{pmatrix} 1 & 0 \\ 0 & 1 \end{pmatrix} \quad , \quad (A.3a)$$

and

$$\sin\left(\frac{\varphi S^\alpha}{\hbar}\right) = \frac{2}{\hbar} \sin\left(\frac{\varphi}{2}\right) S^\alpha \quad . \quad (A.3b)$$

The commutation relations between the three spin-components read

$$[S^\alpha, S^\beta] = i\hbar\epsilon_{\alpha\beta\gamma}S^\gamma \quad , \quad (A.4)$$

where  $[A, B] \equiv AB - BA$ ,  $\epsilon_{\alpha\beta\gamma}$  is the totally antisymmetric unit tensor ( $\epsilon_{xyz} = \epsilon_{yzx} = \epsilon_{zxy} = 1$ ,  $\epsilon_{\alpha\beta\gamma} = -\epsilon_{\beta\alpha\gamma} = -\epsilon_{\gamma\beta\alpha} = -\epsilon_{\alpha\gamma\beta}$ ,  $\epsilon_{\alpha\alpha\gamma} = 0$ ) and the summation convention is assumed.

Rotation of the spin about an angle  $\varphi$  around the axis  $\beta$  gives

$$S^\alpha(\varphi, \beta) \equiv e^{i\varphi S^\beta/\hbar} S^\alpha e^{-i\varphi S^\beta/\hbar} = S^\alpha \cos \varphi + \epsilon_{\alpha\beta\gamma} S^\gamma \sin \varphi \quad . \quad (A.5)$$

Of particular interest to quantum computing are rotations about  $\pi/2$  around the  $x$  and  $y$ -axis defined by

$$X \equiv e^{i\pi S^x/2\hbar} = \frac{1}{\sqrt{2}} \begin{pmatrix} 1 & i \\ i & 1 \end{pmatrix} \quad , \quad (A.6a)$$

and

$$Y \equiv e^{i\pi S^y/2\hbar} = \frac{1}{\sqrt{2}} \begin{pmatrix} 1 & 1 \\ -1 & 1 \end{pmatrix} \quad . \quad (A.6b)$$

The inverse of a rotation  $Z$  will be denoted as  $\bar{Z}$  and if more than one spin is involved a subscript will be attached. With our convention  $\langle \uparrow | \bar{Y} S^x Y | \uparrow \rangle = -1/2$  so that a positive angle corresponds to a rotation in the clock-wise direction.

Another basic operation is the Walsh-Hadamard transform  $W$  which rotates the state  $|\uparrow\rangle$  into  $(|\downarrow\rangle + |\uparrow\rangle)/\sqrt{2}$  (up to an irrelevant phase factor), i.e. the uniform superposition state. In terms of elementary rotations the Walsh-Hadamard transform reads

$$W = X^2 \bar{Y} = Y X^2 = -\bar{X}^2 \bar{Y} = -Y \bar{X}^2 = \frac{i}{\sqrt{2}} \begin{pmatrix} 1 & 1 \\ 1 & -1 \end{pmatrix} \quad , \quad (A.7)$$

For example

$$W|\uparrow\rangle = W \begin{pmatrix} 1 \\ 0 \end{pmatrix} = \frac{i}{\sqrt{2}} \begin{pmatrix} 1 \\ 1 \end{pmatrix} \quad . \quad (A.8)$$

We now consider the time evolution of a single spin subject to a constant magnetic field along the  $z$ -axis and a RF-field along the  $x$ -axis, i.e. the elementary model of NMR. The TDSE reads

$$i\hbar \frac{\partial}{\partial t} |\Phi(t)\rangle = -[H_0 S^z + H_1 S^x \sin \omega t] |\Phi(t)\rangle \quad , \quad (A.9)$$

where  $|\Phi(t=0)\rangle$  is the initial state of the two-state system and we have set the phase in (3) to zero for notational convenience. Substituting  $|\Phi(t)\rangle = e^{it\omega_0 S^z/\hbar} |\Psi(t)\rangle$  yields

$$i\hbar \frac{\partial}{\partial t} |\Psi(t)\rangle = -[(H_0 - \omega_0) S^z + H_1 S^x \sin \omega t \cos \omega_0 t + H_1 S^y \sin \omega t \sin \omega_0 t] |\Psi(t)\rangle \quad , \quad (A.10)$$

which upon choosing  $\omega_0 = H_0$  can be written as

$$i\hbar \frac{\partial}{\partial t} |\Psi(t)\rangle = -H_1 [S^x \sin \omega t \cos \omega_0 t + S^y \sin \omega t \sin \omega_0 t] |\Psi(t)\rangle \quad . \quad (A.11)$$

At resonance, i.e.  $\omega = H_0$ , we find

$$i\hbar \frac{\partial}{\partial t} |\Psi(t)\rangle = -\frac{H_1}{2} [S^y + S^x \sin 2H_0 t - S^y \cos 2H_0 t] |\Psi(t)\rangle . \quad (A.12)$$

Assuming that the effects of the higher harmonic terms (i.e. the terms in  $\sin 2H_0 t$  and  $\cos 2H_0 t$ ) are small [34] we obtain

$$i\hbar \frac{\partial}{\partial t} |\Psi(t)\rangle \approx -\frac{H_1}{2} S^y |\Psi(t)\rangle , \quad (A.13)$$

which is easily solved to give

$$|\Psi(t)\rangle \approx e^{itH_1S^y/2\hbar} |\Psi(t=0)\rangle , \quad (A.14)$$

so that the overall action of an RF-pulse of duration  $\tau$  can be written as

$$|\Phi(t+\tau)\rangle \approx e^{i\tau H_0 S^z/\hbar} e^{i\tau H_1 S^y/2\hbar} |\Phi(t)\rangle . \quad (A.15)$$

From (A.15) it follows that application of an RF-pulse of “power”  $\tau H_1 = \pi$  will have the effect of rotating the spin by an angle of  $\pi/2$  about the  $y$ -axis. For example

$$\begin{aligned} e^{i\tau H_0 S^z/\hbar} e^{i\pi S^y/2\hbar} |\uparrow\rangle &= e^{i\tau H_0 S^z/\hbar} \left[ \cos \frac{\pi}{4} \begin{pmatrix} 1 & 0 \\ 0 & 1 \end{pmatrix} + i \sin \frac{\pi}{4} \begin{pmatrix} 0 & -i \\ i & 0 \end{pmatrix} \right] \begin{pmatrix} 1 \\ 0 \end{pmatrix} \\ &= \frac{1}{\sqrt{2}} e^{i\tau H_0 S^z/\hbar} \begin{pmatrix} 1 \\ -1 \end{pmatrix} \\ &= \frac{1}{\sqrt{2}} \begin{pmatrix} e^{i\tau H_0/2} \\ -e^{-i\tau H_0/2} \end{pmatrix} . \end{aligned} \quad (A.16)$$

In this rotated state the expectation values of the spin components are given by

$$\langle \uparrow | e^{-i\pi S^y/2\hbar} e^{-i\tau H_0 S^z/\hbar} S^x e^{i\tau H_0 S^z/\hbar} e^{i\pi S^y/2\hbar} | \uparrow \rangle = -\hbar \cos \tau H_0 , \quad (A.17a)$$

$$\langle \uparrow | e^{-i\pi S^y/2\hbar} e^{-i\tau H_0 S^z/\hbar} S^y e^{i\tau H_0 S^z/\hbar} e^{i\pi S^y/2\hbar} | \uparrow \rangle = -\hbar \sin \tau H_0 , \quad (A.17b)$$

$$\langle \uparrow | e^{-i\pi S^y/2\hbar} e^{-i\tau H_0 S^z/\hbar} S^z e^{i\tau H_0 S^z/\hbar} e^{i\pi S^y/2\hbar} | \uparrow \rangle = 0 , \quad (A.17c)$$

showing that the time of the RF-pulse also affects the projection of the spin on the  $x$  and  $y$  axis.

It is instructive to derive the TDSE that corresponds to approximation (A.15). Taking the derivative of (A.15) with respect to  $t$  we obtain

$$i\hbar \frac{\partial}{\partial t} |\Phi(t)\rangle = -H_0 S^z - \frac{H_1}{2} [S^x \sin H_0 t + S^y \cos H_0 t] |\Phi(t)\rangle , \quad (A.18)$$

telling us that the approximate solution (A.15) is the exact solution for an RF field rotating in space [34]. The fact that the application of an RF-pulse does not exactly correspond to a simple rotation in spin space may well be important for applications of NMR techniques to QC's.

Finally we note that our choice of using a “ $\sin \omega t$ ” instead of “ $\cos \omega t$ ” [34] to couple the spin to the RF-field merely leads to a phase shift. In the former case rotating the spin around the  $x$ -axis requires a pulse along the  $y$ -axis, whereas in the latter the pulse should be applied along the  $x$ -axis [34].

## Appendix B: Basic operations

Below we list a number of identities that are useful to compute by hand the action of the sequences appearing above. The convention adopted in this paper is that

$$|0\rangle = |\uparrow\rangle = \begin{pmatrix} 1 \\ 0 \end{pmatrix} \quad ; \quad |1\rangle = |\downarrow\rangle = \begin{pmatrix} 0 \\ 1 \end{pmatrix} \quad . \quad (B.1)$$

A straightforward calculation yields:

$$X|0\rangle = \frac{1}{\sqrt{2}}(|0\rangle + i|1\rangle) \quad , \quad X|1\rangle = \frac{1}{\sqrt{2}}(i|0\rangle + |1\rangle) \quad , \quad (B.2a)$$

$$\bar{X}|0\rangle = \frac{1}{\sqrt{2}}(|0\rangle - i|1\rangle) \quad , \quad \bar{X}|1\rangle = \frac{1}{\sqrt{2}}(-i|0\rangle + |1\rangle) \quad , \quad (B.2b)$$

$$Y|0\rangle = \frac{1}{\sqrt{2}}(|0\rangle - |1\rangle) \quad , \quad Y|1\rangle = \frac{1}{\sqrt{2}}(|0\rangle + |1\rangle) \quad , \quad (B.3a)$$

$$\bar{Y}|0\rangle = \frac{1}{\sqrt{2}}(|0\rangle + |1\rangle) \quad , \quad \bar{Y}|1\rangle = \frac{1}{\sqrt{2}}(-|0\rangle + |1\rangle) \quad , \quad (B.3b)$$

$$Y \left[ \frac{1}{\sqrt{2}}(|0\rangle - |1\rangle) \right] = -|1\rangle \quad , \quad Y \left[ \frac{1}{\sqrt{2}}(|0\rangle + |1\rangle) \right] = |0\rangle \quad , \quad (B.4a)$$

$$\bar{Y} \left[ \frac{1}{\sqrt{2}}(|0\rangle - |1\rangle) \right] = |0\rangle \quad , \quad \bar{Y} \left[ \frac{1}{\sqrt{2}}(|0\rangle + |1\rangle) \right] = |1\rangle \quad , \quad (B.4b)$$

$$XX|0\rangle = i|1\rangle \quad , \quad XX|1\rangle = i|0\rangle \quad , \quad (B.5a)$$

$$YY|0\rangle = -|1\rangle \quad , \quad YY|1\rangle = |0\rangle \quad , \quad (B.5b)$$

$$XY|0\rangle = \frac{e^{-i\pi/4}}{\sqrt{2}}(|0\rangle - |1\rangle) \quad , \quad XY|1\rangle = \frac{e^{+i\pi/4}}{\sqrt{2}}(|0\rangle + |1\rangle) \quad , \quad (B.6a)$$

$$\bar{X}Y|0\rangle = \frac{e^{+i\pi/4}}{\sqrt{2}}(|0\rangle - |1\rangle) \quad , \quad \bar{X}Y|1\rangle = \frac{e^{-i\pi/4}}{\sqrt{2}}(|0\rangle + |1\rangle) \quad , \quad (B.6b)$$

$$X\bar{Y}|0\rangle = \frac{e^{+i\pi/4}}{\sqrt{2}}(|0\rangle + |1\rangle) \quad , \quad X\bar{Y}|1\rangle = \frac{e^{-i\pi/4}}{\sqrt{2}}(-|0\rangle + |1\rangle) \quad , \quad (B.6c)$$

$$\bar{X}\bar{Y}|0\rangle = \frac{e^{-i\pi/4}}{\sqrt{2}}(|0\rangle + |1\rangle) \quad , \quad \bar{X}\bar{Y}|1\rangle = \frac{e^{+i\pi/4}}{\sqrt{2}}(-|0\rangle + |1\rangle) \quad , \quad (B.6d)$$

$$\bar{Y}XY|0\rangle = e^{-i\pi/4}|0\rangle \quad , \quad \bar{Y}XY|1\rangle = e^{+i\pi/4}|1\rangle \quad , \quad (B.7a)$$

$$\bar{Y}X\bar{Y}|0\rangle = e^{+i\pi/4}|1\rangle \quad , \quad \bar{Y}X\bar{Y}|1\rangle = -e^{-i\pi/4}|0\rangle \quad , \quad (B.7b)$$

$$Y\bar{X}\bar{Y}|0\rangle = e^{-i\pi/4}|0\rangle \quad , \quad Y\bar{X}\bar{Y}|1\rangle = e^{+i\pi/4}|1\rangle \quad , \quad (B.7c)$$

$$W = X^2\bar{Y} = YX^2 = -\bar{X}^2Y = -Y\bar{X}^2 \quad , \quad (B.8a)$$

$$W|0\rangle = \frac{i}{\sqrt{2}}(|0\rangle + |1\rangle) \quad , \quad W|1\rangle = \frac{i}{\sqrt{2}}(|0\rangle - |1\rangle) \quad , \quad (B.8b)$$

$$W^2|0\rangle = -|0\rangle \quad , \quad W^2|1\rangle = -|1\rangle \quad . \quad (B.8c)$$

## References

1. J.A. Jones, and M. Mosca, "Implementation of a quantum algorithm on a nuclear magnetic resonance quantum computer", *J. Chem. Phys.* **109**, 1648 - 1653 (1998).
2. J.A. Jones, M. Mosca, and R.H. Hansen, "Implementation of a quantum search algorithm on a quantum computer", *Nature (London)* **393**, 344 - 346 (1998).
3. I.L. Chuang, L.M.K. Vandersypen, Xinlan Zhou, D.W. Leung, and S. Lloyd, "Experimental realization of a quantum algorithm", *Nature* **393**, 143 - 146 (1998).
4. I.L. Chuang, N. Gershenfeld, and M. Kubinec, "Experimental implementation of Fast Quantum Searching", *Phys. Rev. Lett.* **80**, 3408 - 3411 (1998).
5. C. Bennett, and G. Brassard, "The Dawn of a New Era for Quantum Cryptography: The Experimental Prototype is Working", *SIGACT News* **20**, 78 - 82 (1989).
6. C. Bennett, F. Bessette, G. Brassard, L.G. Salvail, and J. Smolin, "Experimental Quantum Cryptography", *J. Cryptology* **5**, 3 - 28 (1992).
7. A. Ekert, J. Rarity, P. Tapster, and G. Palma, "Practical Quantum Cryptography Based on Two-Photon Interferometry", *Phys. Rev. Lett.* **69**, 1293 - 1295 (1992).
8. P. Shor, "Algorithms for quantum computation: Discrete logarithms and factoring", in *Proc. 35th Annu. Symp. Foundations of Computer Science*, S. Goldwasser ed., 124 (IEEE Computer Soc., Los Alamitos CA, 1994).
9. I.L. Chuang, R. Laflamme, P.W. Shor, and W.H. Zurek, "Quantum Computers, Factoring and Decoherence", *Science* **230**, 1663 - 1665 (1995).
10. A.Yu. Kitaev, "Quantum measurements and the Abelian stabiliser problem", e-print quant-ph/9511026.
11. L.K. Grover, "A fast quantum mechanical algorithm for database search", in *Proc. of the 28th Annual ACM Symposium of Theory of Computing* (ACM, Philadelphia 1996).
12. L.K. Grover, "Quantum Computers can search arbitrary large databases by a single query", *Phys. Rev. Lett.* **79**, 4709 - 4712 (1997).
13. L.K. Grover, "Quantum Computers can search rapidly by using almost any transformation", *Phys. Rev. Lett.* **80**, 4329 - 4332 (1998).
14. D. Aharonov, "Quantum Computation", e-print quant-ph/9812037.
15. N.J. Cerf, and S.E. Koonin, "Monte Carlo simulation of quantum computation", *Mathematics and Computers in Simulation* **47**, 143 - 152 (1998).
16. C. Zalka, "Simulating quantum systems on a quantum computer", *Proc. R. Soc. London* **A454**, 313 - 322 (1998).
17. B.M. Terhal, and S.P. DiVincenzo, "On the problem of equilibration and the

computation of correlation functions on a quantum computer”, e-print quant-ph/9810063.

18. H. De Raedt, A.H. Hams, K. Michielsen, S. Miyashita, and K. Saito, “Quantum Statistical Mechanics on a Quantum Computer”, subm. to *Prog. Theor. Phys.*
19. R.P. Feynman, “Simulating Physics with Computers”, *Int. J. Theor. Phys.* **21**, 467 - 488 (1982).
20. D. Deutsch, and R. Jozsa, “Rapid solution of problems by quantum computation”, *Proc. R. Soc. Lond. A* **439**, 553 - 558 (1992).
21. D. Collins, K.W. Kim, and W.C. Holton, “Deutsch-Jozsa algorithm as a test of quantum computation”, *Phys. Rev. A* **58**, R1633 - R1636 (1998).
22. We use a notation that closely resembles the symbols in the QCE’s graphical user interface.
23. H. De Raedt, “Product Formula Algorithms for Solving the Time-Dependent Schrödinger Equation”, *Comp. Phys. Rep.* **7**, 1 - 72 (1987).
24. J. Huyghebaert, and H. De Raedt, “Product formula methods for time-dependent Schrödinger problems”, *J. Phys. A:Math. Gen.* **23**, 5777 (1990).
25. M. Suzuki, “General Decomposition Theory of Ordered Exponentials”, *Proc. Japan Acad.* **69**, Ser. B 161 - 166 (1993).
26. P. de Vries, and H. De Raedt “Solution of the time-dependent Schrödinger equation for two-dimensional spin-1/2 Heisenberg systems”, *Phys. Rev. B* **47**, 7929 - 7937 (1993).
27. M. Suzuki, S. Miyashita, and A. Kuroda, “Monte Carlo Simulation of Quantum Spin Systems. I”, *Prog. Theor. Phys.* **58**, 1377 - 1387 (1977).
28. H. De Raedt, and B. De Raedt, “Applications of the Generalized Trotter Formula”, *Phys. Rev. A* **28**, 3575 - 3580 (1983).
29. M. Suzuki, “Decomposition Formulas of Exponential Operators and Lie Exponentials with some Applications to Quantum Mechanics and Statistical Physics” *J. Math. Phys.* **26**, 601 - 612 (1985).
30. H. De Raedt and K. Michielsen, “Algorithm to Solve the Time-Dependent Schrödinger Equation for a Charged Particle in an Inhomogeneous Magnetic Field: Application to the Aharonov-Bohm Effect”, *Comp. in Phys.* **8**, 600 - 607 (1994).
31. M. Suzuki, “General Nonsymmetric Higher-Order Decomposition of Exponential Operators and Symplectic Integrators” *J. Phys. Soc. Jpn.* **61**, 3015 - 3019 (1995).
32. R. Cleve, A. Ekert, C. Macciavello, and M. Mosca, “Quantum algorithms revisited”, *Proc. R. Soc. Lond. A* **454**, 339 - 354 (1998).
33. C.P. Slichter, “Principles of Magnetic Resonance”, (Springer, Berlin, 1990).
34. G. Baym, “Lectures on Quantum Mechanics”, (W.A. Benjamin, Reading MA, 1974).

35. We follow the convention used earlier in this paper, i.e. the one used in [3] and therefore deviate from the notation used in [4].
36. H. De Raedt, A.H. Hams, K. Michielsen, S. Miyashita, and K. Saito, “Quantum Spins Dynamics and Quantum Computation”, subm. to J. Phys. Soc. Jpn..

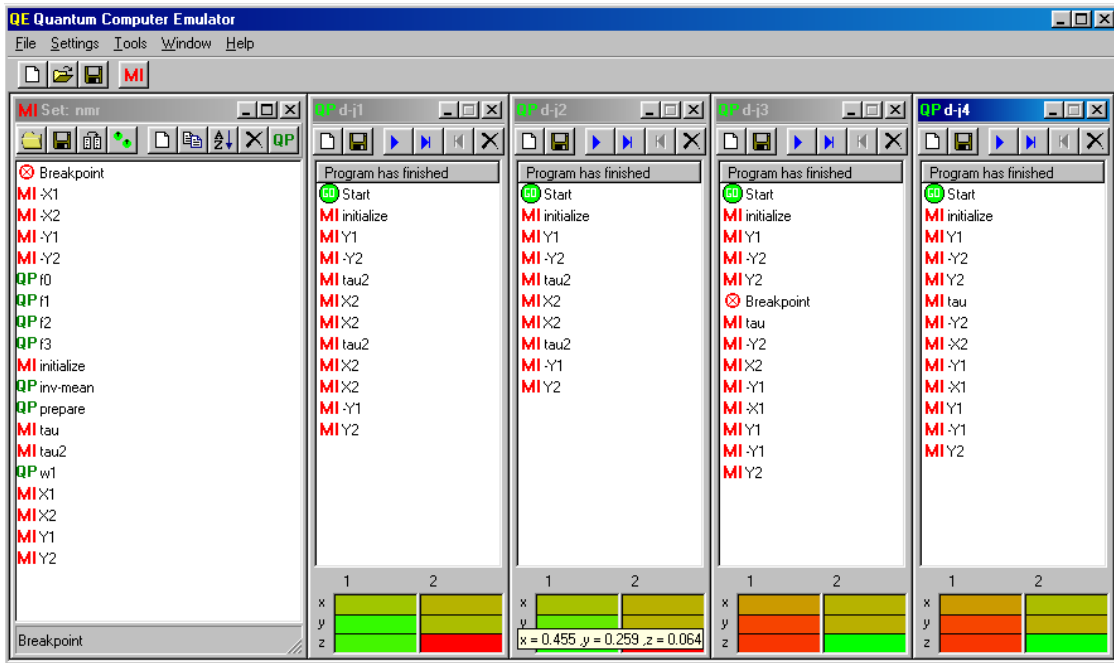


Fig.1. Picture of the Quantum Computer Emulator showing a window with a set of micro instructions implementing an NMR quantum computer and windows with four Deutsch-Jozsa programs (d-j1, ..., d-j4), one for each function ( $f_1(x)$ , ...,  $f_4(x)$ ) listed in Table 1. The final state of the QC, i.e. the expectation value of the qubits (spin operators), is shown at the bottom of each program window (green =  $|0\rangle$ , red =  $|1\rangle$ ). The numerical values appear if the cursor moves over the qubit area.

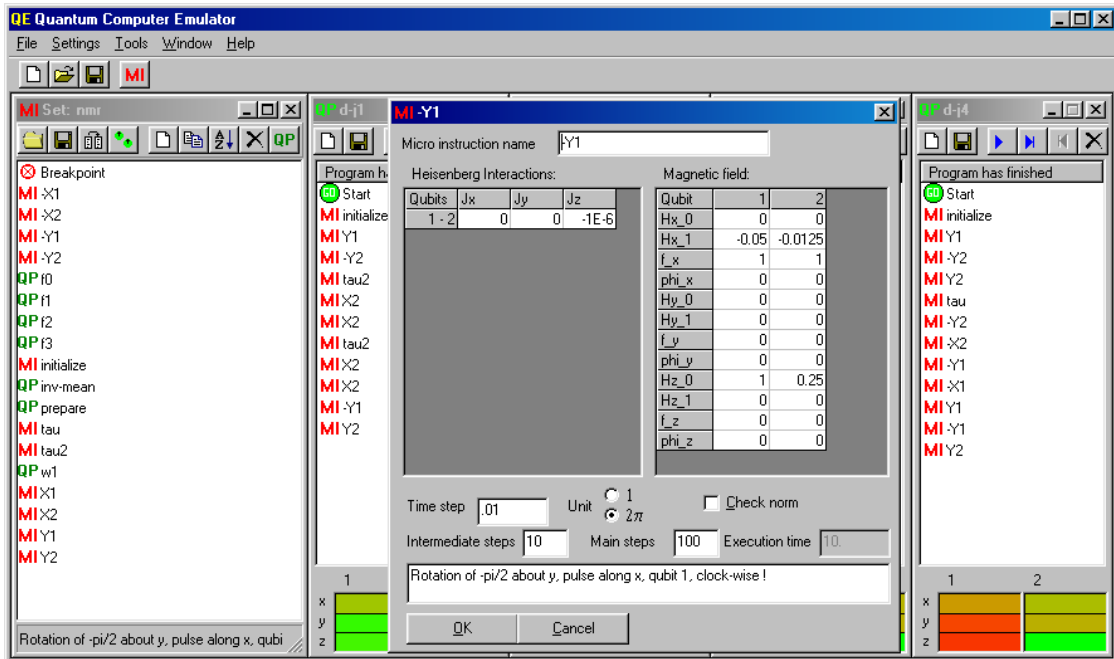


Fig.2. Picture of the Quantum Computer Emulator showing a window with a set of micro instructions implementing an ideal quantum computer and windows with four Deutsch-Jozsa programs ( $d-j1, \dots, d-j4$ ), one for each function ( $f_1(x), \dots, f_4(x)$ ) listed in Table 1. Also shown is a window for editing micro instructions, which appears by double-clicking on a micro instruction ( $x2$  in this example). The final state of the quantum computer, i.e. the expectation value of the qubits (spin operators), is shown at the bottom of each program window (green =  $|0\rangle$ , red =  $|1\rangle$ ). In this ideal case the expectation values are either zero or one.

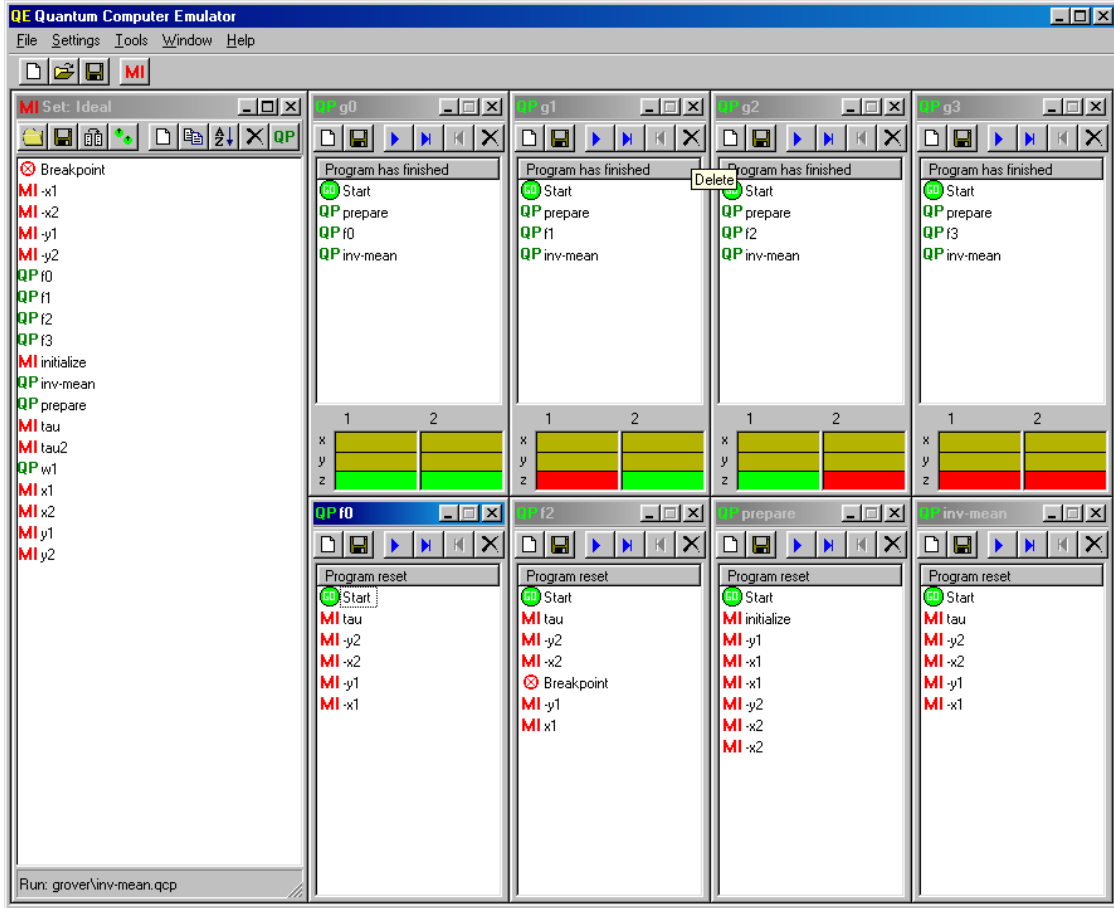


Fig.3. Picture of the Quantum Computer Emulator showing a window with a set of micro instructions for an ideal two-qubit quantum computer and windows with quantum programs implementing Grover's database search for the four different cases  $g_0(x)$  ( $g_0$ ), ...,  $g_3(x)$  ( $g_3$ ). This example also shows the use of quantum programs as micro instructions in other quantum programs. The final state of the QC, i.e. two qubits shown at the bottom of each program, gives the location (in binary representation) of the item in the database.

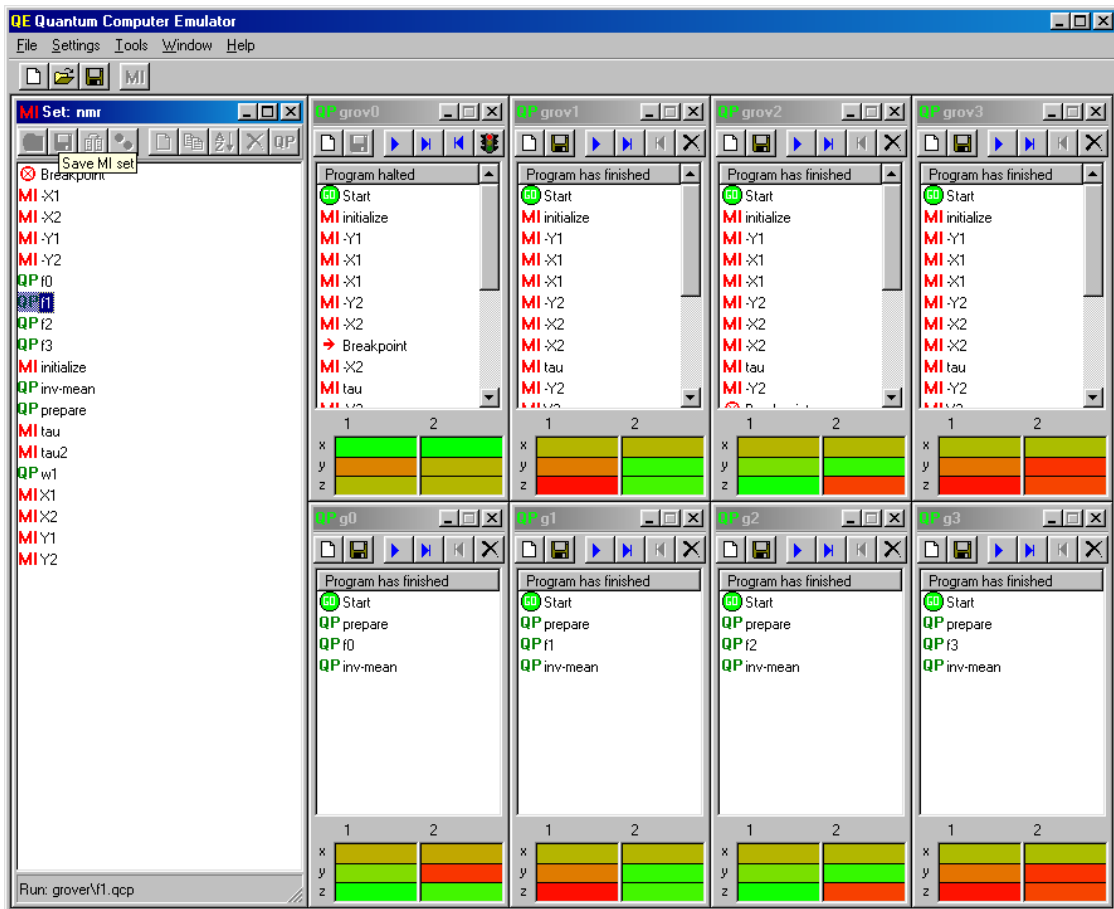


Fig.4. Picture of the Quantum Computer Emulator showing a window with a set of micro instructions for the two-qubit NMR quantum computer and windows with quantum programs implementing Grover's database search for the four different cases  $g_0(x), \dots, g_3(x)$ , using the basic MI's (grov0, ..., grov3) and calls to other quantum programs (g0, ..., g3). The final state of the quantum computer, i.e. two qubits shown at the bottom of each program, gives the location (in binary representation) of the item in the database. This final state is no longer a pure basis state but as the weight of basis state corresponding the location of the item is by far the largest the correct answer is easy to infer.